A Statistical Method for Improving Continental Shelf and Nearshore Marine Climate Predictions

ERIC C. J. OLIVER

Institute for Marine and Antarctic Studies, University of Tasmania, Hobart, Tasmania, Australia

NEIL J. HOLBROOK

Institute for Marine and Antarctic Studies, and Australian Research Council Centre of Excellence for Climate System Science, University of Tasmania, Hobart, Tasmania, Australia

(Manuscript received 21 February 2013, in final form 24 May 2013)

ABSTRACT

Spatially and temporally homogeneous measurements of ocean temperature variability at high resolution on the continental shelf are scarce. Daily estimates of large-scale ocean properties are readily available from global ocean reanalysis products. However, the ocean models that underpin these reanalysis products tend not to have been designed for the simulation of complex coastal ocean variability. Hence, across-shelf values are often poorly represented. This study involved developing a statistical approach to more accurately and robustly represent SST on the continental shelf informed by large-scale satellite observations and reanalysis data or model output. Using the southeastern Australian shelf region as a case study, this paper demonstrates that this statistical model approach generates more accurate estimates of the inshore SST using (i) offshore SST from Bluelink Reanalysis (BRAN) and (ii) the statistical relationship between inshore and offshore SST in observations from the Advanced Very High Resolution Radiometer. SST is separated into the mean, seasonal cycle, and residual variability, and separate models are developed for each component. The offshore locations used to inform the model are determined by taking into account (i) the quality of BRAN at each location, (ii) the strength between the inshore and offshore variability, and (iii) the proximity of the inshore and offshore locations. Model predictions are made for the continental shelf around southeastern Australia. The role of the mean circulation in providing connectivity between the shelf and the offshore regions is discussed, and how this information can be used to better inform the choice of model predictor locations, leading to a hybrid statistical–connectivity model.

1. Introduction

Ocean climate observations (e.g., temperature, salinity, nutrients, flow speeds, and directions) are typically sparse in space and time across the globe. Long-term moored observing stations and/or repeat observational transects tend to be costly and are not easily resourced. This is not only true for the deep ocean but also in nearshore regions across the continental shelf. Satellite-observing instruments such as the Advanced Very High Resolution Radiometer (AVHRR) mounted on orbiting satellites provide high-resolution repeat measurements of sea surface temperature (SST) along track. Unfortunately, these instruments lack a temporal sample rate high enough to consistently capture high-resolution SST variability on daily to weekly time scales, for example, variability resulting from mesoscale eddies or synoptic weather forcing. Fixed measurement stations and moorings can provide location-specific observations with high sample rates but, unless there are many such instruments as part of a large network, lack the spatial coverage or homogeneity in both space and time. Global ocean models and reanalysis data can also be valuable tools and products to help synthesize our understanding but are typically insufficient on their own to capture the physical processes that govern SST variability on the continental shelf, since they tend to be conditioned to represent the large-scale ocean circulation.

One method for synthesizing irregularly spaced observations is objective mapping, which takes account of relevant space and time signal and noise scales. For

Corresponding author address: Eric C. J. Oliver, Institute for Marine and Antarctic Studies, University of Tasmania, Private Bag 129, Hobart, TAS 7001, Australia.
E-mail: eric.oliver@utas.edu.au

DOI: 10.1175/JTECH-D-13-00052.1

example, Holbrook and Bindoff (2000) generated a dataset of uniformly gridded upper-ocean temperatures using an objective mapping technique that takes advantage of the strong vertical correlations in ocean temperature data to minimize the cost. Ridgway et al. (2002) interpolated irregularly spaced ocean temperature and salinity observations onto a regular grid using a loess filter that takes into account data at neighboring vertical levels as well as the influence of bathymetry and land barriers.

Here, however, rather than interpolating existing data, we wish to improve global ocean model estimates of the marine climate across the shelf. Downscaling is an approach often used to perform such a task. It provides the link between the large-scale state of some variable, for which there is typically coarsely gridded information, and the smaller-scale state of that or another variable, for which there is no accurate scale-relevant information (von Storch et al. 1993; Benestad et al. 2008). For example, global climate models provide reasonably accurate predictions of global surface air temperature at coarse spatial resolutions (e.g., 1°–2° in latitude and longitude) but cannot reliably predict smaller-scale variations due to the presence of unresolved features such as clouds or steep orography. There are two approaches to downscaling: dynamical downscaling and statistical downscaling (e.g., Murphy 1999).

Dynamical downscaling nests one or more fine-resolution general circulation model(s) within the domain of a coarse-resolution circulation model. Dynamical downscaling allows for important physical processes to be resolved at high resolution in the part of the domain of interest, while the remainder of the domain is represented using the coarse-resolution large-scale model. Dynamical downscaling is commonly applied to global climate model output (e.g., Giorgi 1990; Christensen et al. 1998; Murphy 1999; Corney et al. 2010), but it has also been used in an ocean-only context using nested grids (e.g., Oey and Chen 1992; Guo et al. 2003; Oliver 2011). Alternatively, a heterogeneous grid spacing can allow for specific regions to be resolved more finely than others, within the same grid [e.g., the Australian marine region (Oke et al. 2008), or the tropical Pacific Ocean (Zhang et al. 2010)]. An extension of dynamical downscaling is telescoping, in which multiple nested models are used to focus in on a particular region of interest (e.g., Christensen et al. 1998; Guo et al. 2003; Trapp et al. 2007). For example, Trapp et al. (2007) used global 2.5° × 2.5°–resolution National Center for Atmospheric Research (NCAR) atmospheric reanalysis data as the coarse-scale information and nested a higher-resolution (~55 km) regional climate model within a domain covering the continental United States. A convection-permitting model, with a horizontal resolution of less than 4 km, was further nested within the regional climate model to allow for convective storm behavior to be resolved over small-scale local domains. The most significant downside to dynamical downscaling is that the required circulation models are costly to develop, implement, and validate.

Statistical downscaling is an alternative approach that takes the observed statistical relationship between the large-scale variability (e.g., large-scale general circulation features) and local variability (e.g., station measurements)—a relationship that depends on processes not resolved by coarse climate models—and uses it to "downscale" climate model output and provide predictions of local variability at some point location. One of the simplest approaches is a multivariate linear regression model in which the local variability is regressed onto a set of predictors taken from the large-scale dataset (e.g., Hellstrom et al. 2001; Huth 2002). More complex methods include the use of principal components or canonical correlations analysis (e.g., von Storch and Zwiers 2002; Huth 2002), stochastic weather generators (e.g., Wilks 1999; Palutikof et al. 2002; Qian et al. 2002), and neural networks (e.g., Zorita and von Storch 1999), among others. Statistical downscaling has primarily been used to downscale climate for the terrestrial environment (e.g., Wilby et al. 1998) and has not been used as extensively for the marine environment; existing downscaling studies for oceanic variables have primarily focused on ocean wave climate (e.g., Wang et al. 2010). In general, statistical downscaling is more computationally efficient than dynamical downscaling, but it lacks the dynamical consistency between variables provided by the latter approach.

Our focus here, however, is not strictly about statistical downscaling per se, but rather about what we would call "statistical boundary scaling." Given the nature of the oceanographic climate problem, the approach presented in this paper does not scale coarse predictions to a finer resolution over the same domain. Instead, we use accurate and robust ocean data from the larger-scale geographic domain—specifically, deeper ocean points proximal to our shelf region of interest—to provide estimates in the domain where the ocean model performs poorly (here, the coastal ocean) based on the observed relationship between those two domains. Unlike statistical downscaling, the statistical boundary-scaling approach presented in this paper does not relate the local finescale variability to the local coarse-scale variability; rather, it relates the local coastal ocean variability to the nonlocal open-ocean variability. We are careful here to detail our approach thoroughly, and contend that this approach is likely to have utility for application more generally to coastal scaling problems outside of the

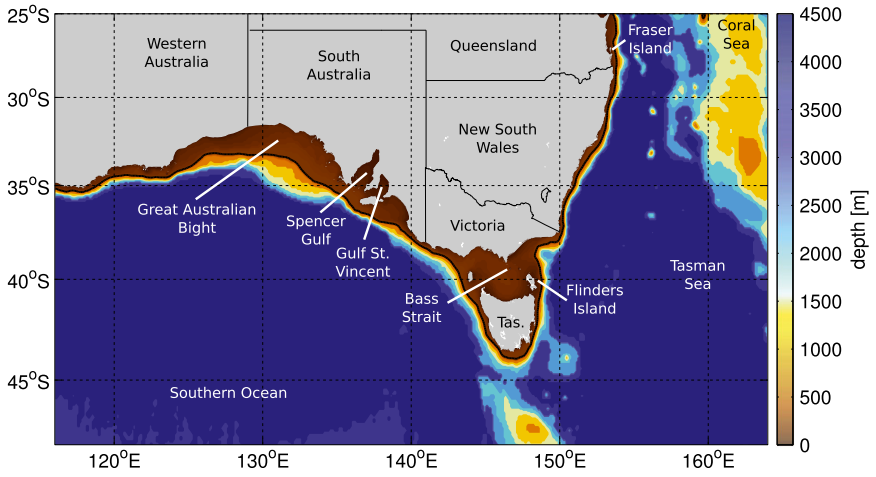

FIG. 1. The domain and bathymetry of southern and southeastern Australia waters used for the statistical boundary-scaling model along with named locations mentioned in this study. Bathymetric contours were calculated from the OFAM grid. The black line is the 200-m-depth contour.

Australian context, which we use here as a case study example of its potential.

Australia has over 35 000 km of coastline and nearly 85% of the population lives within 50 km of the sea (ABS 2001). These marine-related and coastal climate issues are particularly important for Australia, given their proximity to people, its biodiversity and resources (ecosystem services), and amenity. The Ocean Forecasting Australia Model (OFAM) provides the highest-resolution model information available for short-term (7 days) ocean forecasts at an approximate 10-km scale for the ocean environment surrounding Australia. Further, the Bluelink Reanalysis (BRAN) product provides ocean-reanalyzed daily estimates of ocean variability over the 1992–2008 satellite-observing period using the data-assimilative eddy-resolving OFAM, used primarily for ocean and climate diagnostic studies. BRAN reproduces well the large-scale circulation around Australia. For example, the volume transport of the Indonesian Throughflow, the Leeuwin Current, the South Australian Current, and the eddy-rich East Australian Current (EAC) are all well captured (Oke et al. 2008; Schiller et al. 2008). However, since OFAM is designed for the primary purpose of modeling features of the open-ocean circulation rather than the bounding coastal and shelf regions, the BRAN output in space and time tends to evaluate poorly against available across-shelf observations in contrast to the open ocean, where BRAN performs very well. For example, nearshore daily SSTs have been shown to be poorly represented by BRAN, especially along the coast of southeast Australia (Hobday et al. 2011).

To summarize our approach tested here in the Australian context, separate model components are developed for the mean SST, the SST seasonal cycle, and the residual SST variability across southeast and southern Australian marine waters (domain shown in Fig. 1). The model parameters for each component are determined from the observed relationships between AVHRR SSTs on the continental shelf and offshore. For example, the residual component is simply a linear regression of nonseasonal shelf SST variability onto nonseasonal offshore SST variability. The model components are then informed by estimates of offshore SST from BRAN to provide daily estimates of inshore SST on a $^1/_{10}°$ horizontal grid. The statistical SST predictions are then evaluated against observed SSTs. For each location on the continental shelf, the offshore predictor location is determined systematically by jointly taking into account issues related to data quality, the relationship between shelf and offshore SST, and proximity. Our physical understanding of the oceanography along with the results indicates that ocean circulation (connectivity) plays an expected role in connecting the shelf and offshore SST. We use this information, based on Lagrangian trajectories of passive particles, to further refine our predictor selection producing a hybrid statistical–connectivity boundary-scaling model.

This paper is organized as follows. The data sources and a preliminary statistical analysis are presented in section 2. The statistical model is described in section 3. In section 4, the model SST estimates are initially evaluated at a point location in Bass Strait and then extended to the entire continental shelf in three regions: (i) Tasmania and Victoria, (ii) the Great Australian Bight, and (iii) New South Wales and southern Queensland. Model refinements, based on a Lagrangian connectivity analysis utilizing the mean circulation information, are

presented in section 5. Conclusions and further work are discussed in section 6.

2. A basic quality assessment of BRAN SSTs

Daily fields of reanalyzed SSTs were obtained from BRAN, version 2.1, for the period 14 October 1992–30 December 2006 and from BRAN, version 2.2, for the period 29 November 2006–13 May 2008. The two datasets were merged by a linearly weighted average over the 30 days of overlap between them, and the combined dataset is referred to hereafter simply as BRAN. Daily BRAN SST fields are denoted $\breve{\mathbf{T}}_t$ and are analyzed on its $^1/_{10}°$-resolution horizontal grid; $\breve{\mathbf{T}}_t$ is an $m \times n$ matrix, where m and n are the number of grid points in the latitudinal and longitudinal directions, respectively, and t is a time index.

Daily fields of observed SSTs were obtained from AVHRR for the period 14 October –13 May 2008 and are defined on a 4-km-resolution grid. Only the nearest AVHRR grid point to each BRAN location is retained, and these fields are denoted $\mathbf{T}_t$ (also an $m \times n$ matrix). We would like to note that while the AVHRR SST observations have been assimilated into BRAN, there is still a large degree of independence between BRAN and AVHRR over the continental shelf because (i) only SST data in water depth greater than 200 m are assimilated (P. Oke 2013, personal communication), and (ii) only 1 day out of every 7 days of SST data is assimilated and therefore, to the extent that we can ignore serial correlation in time, 6 out of every 7 days of SST data are independent (Oke and Schiller 2007).

We now compare $\mathbf{T}_t$ and $\breve{\mathbf{T}}_t$. Assume the time series of observed temperature T_{ijt} at each location (i, j) can be written as

$$T_{ijt} = \overline{T}_{ij} + T^S_{ijt} + T'_{ijt}, \tag{1}$$

where $\overline{T}_{ij}$ is the time mean, T^S_{ijt} is the seasonal cycle, and T'_{ijt} is the residual (nonseasonal) variability. The seasonal cycle is calculated by harmonic regression (see appendix A). The residual is defined to be the variability remaining after removing the mean and seasonal cycle (interannual variability, subseasonal variability, etc.). The same linear decomposition is assumed to hold for $\breve{\mathbf{T}}_t$.

The quality of $\breve{\mathbf{T}}_t$ is measured in terms of how similar its mean, seasonal cycle, and residual components are to those derived from $\mathbf{T}_t$. Separate quality functions—$\overline{\mathbf{Q}}$, $\mathbf{Q}^S$, and $\mathbf{Q}'$—are defined for each component:

$$\overline{Q}_{ij} = 1 - \left| \frac{\breve{\overline{T}}_{ij} - \overline{T}_{ij}}{\overline{T}_{ij} - T_0} \right| \quad \text{(mean)}, \tag{2}$$

$$Q^S_{ij} = \rho(T^S_{ijt}, \breve{T}^S_{ijt}) \quad \text{(seasonal cycle)}, \tag{3}$$

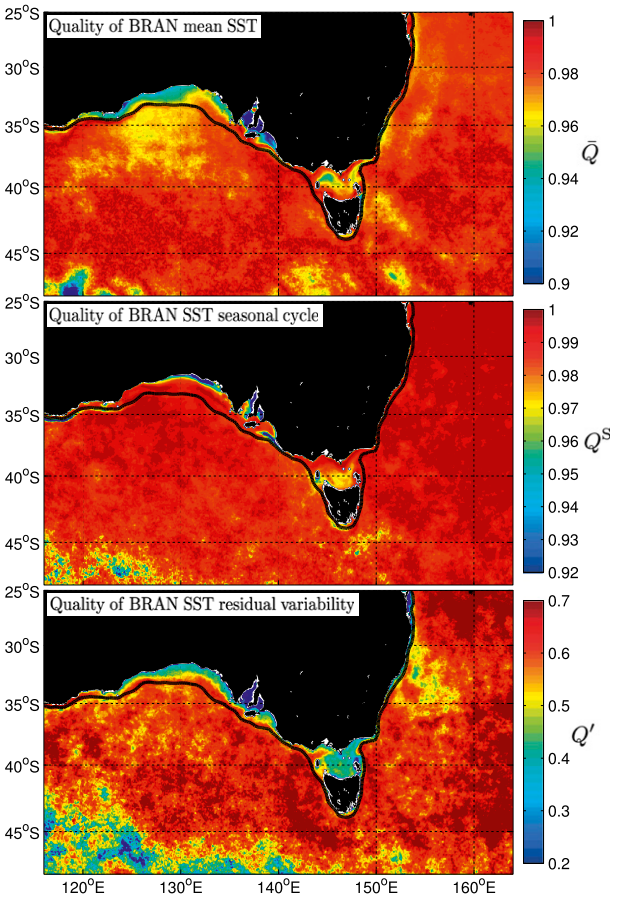

FIG. 2. Comparison of observed and BRAN SST, $\mathbf{T}_t$ and $\breve{\mathbf{T}}_t$, respectively. Colors represent the quality of (top) $\overline{\mathbf{Q}}$, (middle) $\mathbf{Q}^S$, and (bottom) $\mathbf{Q}'$. Definitions of the quality matrices are given by Eqs. (2)–(4). The black line is the 200-m-depth contour.

and

$$Q'_{ij} = \rho(T'_{ijt}, \breve{T}'_{ijt}) \quad \text{(residual)}, \tag{4}$$

respectively, where $|x|$ denotes the absolute value of x, $\rho(x_t, y_t)$ denotes the temporal correlation (e.g., Priestley 1981) between x_t and y_t, and T_0 is a reference temperature (taken to be the freezing point of water, i.e., 0°C). These equations are invariant under a linear transformation of variables (e.g., a change of units). In each case, a quality of one is perfect correspondence between that component of $\breve{\mathbf{T}}_t$ and $\mathbf{T}_t$; values less than one indicate a discrepancy between $\breve{\mathbf{T}}_t$ and $\mathbf{T}_t$.

In general, the quality of the mean, seasonal cycle, and residual variability of $\breve{\mathbf{T}}_t$ is poor over much of the continental shelf (Fig. 2). The value $\overline{\mathbf{Q}}$ is low in Bass Strait, coastal Tasmania, the gulfs of coastal South Australia, and parts of New South Wales; $\mathbf{Q}^S$ is low in the same regions, except coastal New South Wales; and $\mathbf{Q}'$ is low

over nearly the entire continental shelf, including the regions mentioned above, as well as the coasts of New South Wales and Queensland up to the Coral Sea. Note that the quality functions are generally high in deep water (except in regions of strong eddy variability, e.g., the EAC separation and retroflection region and the Antarctic Circumpolar Current). The next section describes the statistical model we developed to predict inshore SST from offshore SST based on optimization criteria.

3. Statistical model

Consider time series of observed SST at an offshore location (i_X, j_X) and an inshore location (i_Y, j_Y):

$$X_t = T_{i_X j_X t} \tag{5}$$

and

$$Y_t = T_{i_Y j_Y t} \tag{6}$$

with offshore and inshore SST from BRAN, $\breve{X}_t$ and $\breve{Y}_t$, respectively, defined analogously. These time series are linearly decomposed into mean SST, SST seasonal cycle, and residual SST variability components [see Eq. (1)]. Separate statistical models have been developed to predict each of these components (submodels) and are explained in sections 3a–c below. The parameters of each submodel are calculated from X_t and Y_t (i.e., the submodels are trained on observed SST). Then a predictor time series $\breve{X}_t$ (i.e., offshore SST from BRAN) informs the model, providing an estimate of the inshore SST denoted $\hat{Y}_t$.

The choices of the offshore and inshore locations—(i_X, j_X) and (i_Y, j_Y), respectively—are in general free. The choice of the inshore location is given by the location at which a prediction of SST is desired. The choice of the offshore location (i.e., the predictor location) is also free, although in section 3d we outline a relatively simple but systematic method of optimally choosing the offshore predictor location, based on jointly maximizing the fundamental relationships between X_t and Y_t.

a. Mean

The time-mean values of X_t and Y_t are scalars and are related linearly by

$$\overline{Y} = a\overline{X}, \tag{7}$$

which leads to a simple expression for the parameter $a = \overline{Y}/\overline{X}$. Given a predictor variable $\breve{X}_t$, the model for the mean of Y_t is

$$\hat{\overline{Y}} = a\breve{\overline{X}} \tag{8}$$

$$= \frac{\overline{Y}}{\overline{X}}\breve{\overline{X}}. \tag{9}$$

b. Seasonal cycle

Assume the seasonal cycle of X_t and Y_t can be written as a sum of K harmonics of the annual cycle:

$$X_t^S = \sum_{k=1}^{K} A_k^X \cos(\omega_k t - \phi_k^X) \tag{10}$$

and

$$Y_t^S = \sum_{k=1}^{K} A_k^Y \cos(\omega_k t - \phi_k^Y), \tag{11}$$

respectively, where A_k, ϕ_k, and ω_k are the amplitude, phase, and frequency of the kth harmonic, respectively. These amplitudes and phases are estimated from X_t and Y_t by harmonic regression (see appendix A for more details).

The amplitude and phase of X_t^S and Y_t^S are related linearly by

$$\left.\begin{aligned} A_k^Y &= \gamma_k A_k^X \\ \phi_k^Y &= \phi_k^X + \Delta_k \end{aligned}\right\} \text{ for } k = 1, \ldots, K, \tag{12}$$

which leads to simple expressions for the parameters γ_k and Δ_k:

$$\left.\begin{aligned} \gamma_k &= A_k^Y / A_k^X \\ \Delta_k &= \phi_k^Y - \phi_k^X \end{aligned}\right\} \text{ for } k = 1, \ldots, K. \tag{13}$$

Given a predictor variable $\breve{X}_t$, the seasonal cycle of Y_t can be predicted by the model

$$\hat{Y}_t^S = \sum_{k=1}^{K} \gamma_k A_k^{\breve{X}} \cos[\omega_k t - (\phi_k^{\breve{X}} + \Delta_k)] \tag{14}$$

$$= \sum_{k=1}^{K} \frac{A_k^Y}{A_k^X} A_k^{\breve{X}} \cos[\omega_k t - (\phi_k^{\breve{X}} + \phi_k^Y - \phi_k^X)]. \tag{15}$$

c. Residual

We plan the residual variability Y_t' using a linear regression model:

$$Y_t' = \beta X_t' + \epsilon_t, \tag{16}$$

where β is the regression coefficient and ϵ_t is an error term representing effects not included in the model.

However, we note that the predictors are imperfect observations of SST and are subject to some measurement error $X'_t = X'^{(\mathrm{tr})}_t + \eta_t$, where $X'^{(\mathrm{tr})}_t$ is the true (unobserved) residual variability and η_t is a noise term representing measurement error. This is known as an ''error in variables'' regression model and, as an estimator of the regression coefficient, the ordinary least squares estimate $\hat{\beta}_{\mathrm{OLS}}$ is biased toward zero (Fuller 1987). An unbiased estimator of the regression coefficient is given by $\hat{\beta} = \lambda^{-1}\hat{\beta}_{\mathrm{OLS}}$, where λ is known as the ''reliability ratio.'' The reliability ratio accounts for the attenuation of the regression coefficient due to measurement error and is given by $\lambda = \sigma_X^{-2}(\sigma_X^2 - \sigma_\eta^2)$, where σ_X^2 and σ_η^2 are the variances of X'_t and η_t, respectively. We take a value of $\sigma_\eta = 0.25$°C for the measurement error on the SST observations (e.g., Oke et al. 2008; Schiller et al. 2008).

Then, given a predictor variable $\breve{X}_t$, the residual variability of Y_t can be predicted by the simple model

$$\hat{Y}'_t = \hat{\beta}\breve{X}'_t \tag{17}$$

and the total inshore SST can be estimated as $\hat{Y}_t$, if desired, from the sum of the submodels

$$\hat{Y}_t = \widehat{\overline{Y}} + \hat{Y}^S_t + \hat{Y}'_t. \tag{18}$$

d. Choice of the predictor location

It is possible to use different predictor locations for each of the individual submodels outlined above. This is desirable, as the mean, seasonal cycle, and residual SST at the same inshore location may be best estimated separately by offshore SST predictors at different locations. For example, the best location from which to predict the mean may not be the best from which to predict the residual variability. There may be good physical reasons why this might be observed, for example, different physical processes operate on different time scales and may lead to differing spatial relationships. We show later that mean circulation (connectivity) can be considered one such physical process.

We note three quantities that may influence the likelihood of a given offshore location providing an accurate prediction of inshore SST. First, the quality matrix **Q** measures the extent to which the variability (or mean, seasonal cycle, etc.) of BRAN is similar to that observed at each point (i, j). The quality matrices were defined for the mean, the seasonal cycle, and the residual components [see Eqs. (2)–(4)]. Second, the strength matrix **S** measures the extent to which the observed variability (or mean, seasonal cycle, etc) is similar between location (i_Y, j_Y) and each location (i, j). The strength matrices for the mean, seasonal cycle, and residual components are defined in a similar way as the quality matrices:

$$\overline{S}_{ij} = 1 - \left| \frac{\overline{T}_{ij} - \overline{T}_{i_Y j_Y}}{\overline{T}_{i_Y j_Y} - T_0} \right| \quad \text{(mean)}, \tag{19}$$

$$S^S_{ij} = \rho(T^S_{ijt}, T^S_{i_Y j_Y t}) \quad \text{(seasonal cycle)}, \tag{20}$$

and

$$S'_{ij} = \rho(T'_{ijt}, T'_{i_Y j_Y t}) \quad \text{(residual)}, \tag{21}$$

where, as above, T_0 is a reference temperature (0°C). The strength matrices are equal to 1 at (i_Y, j_Y) and decrease away from that location. Finally, the localization matrix **R** is an isotropic two-dimensional Gaussian centered on the inshore location (i_Y, j_Y) with a decay scale σ,

$$R_{ij} = \exp\{-[(i - i_Y)^2 + (j - j_Y)^2]/2\sigma^2\}. \tag{22}$$

We postulate that the likelihood of a given offshore location providing an accurate prediction of inshore SST increases with **Q**, **S**, and **R**. A cost matrix **J** has been defined that jointly takes into account the variations of **Q**, **S**, and **R**,

$$J_{ij} = \frac{1}{Q_{ij} S_{ij} R_{ij}}, \tag{23}$$

the minimum of which defines the optimal offshore predictor location. The **Q**, **S**, and **R** matrices have maximum possible values of 1 and thus the cost matrix **J** has a minimum possible value of 1; **J** decreases with (i) the data quality at the possible predictor location, (ii) the strength of the connection between the predictand and the possible predictor location, and (iii) the proximity of the predictand location and the possible predictor location. Equation (23) gives equal weight to the **Q**, **S**, and **R** matrices. Sensitivity tests were performed with relative weighting of the three terms (see appendix B), and it was determined that the results are not strongly sensitive to changes in relative weighting and so we elected to use the simplest model (i.e., equally weighted).

4. Application of the statistical model in southeastern Australia

The statistical model was used to estimate SSTs on the continental shelf in southeastern Australia. First, the model was tested at a point location in Bass Strait (section 4a). Then, the method was applied to the entire southeast Australian continental shelf including Victoria and

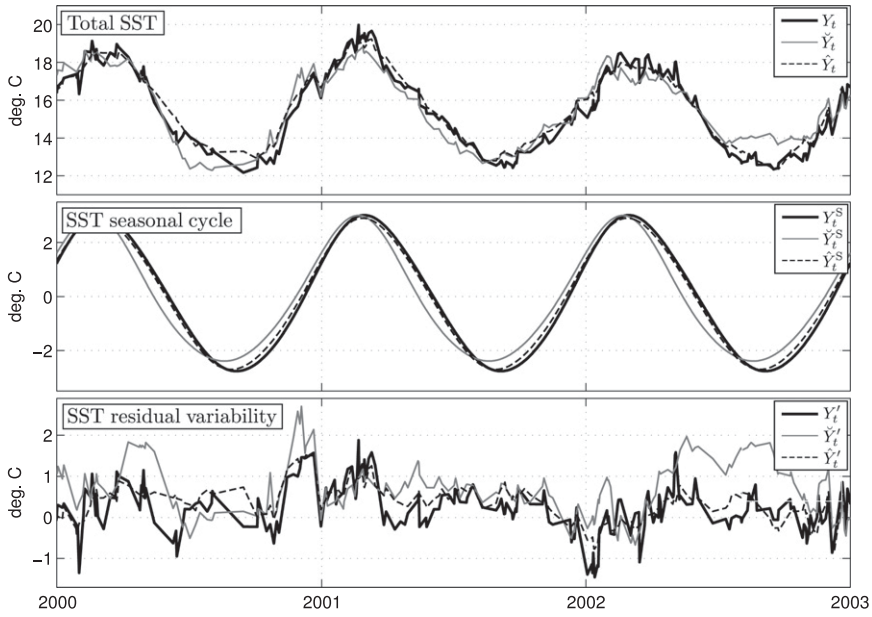

FIG. 3. SST variability at a location (40°S, 147°E) in Bass Strait. Time series of (top) total SST, (middle) seasonal cycle of SST, and (bottom) residual SST from observations (black lines), BRAN (gray lines), and the statistical model prediction (dashed lines). The statistical model is informed by offshore SST from BRAN (see Fig. 4 for locations of inshore and offshore points).

Tasmania, the Great Australian Bight, New South Wales, and southern Queensland (section 4b).

a. Estimating SST at a point location in Bass Strait

Time series of observed SST (Y_t) and BRAN SST ($\breve{Y}_t$) at a location (40°S, 147°E) in Bass Strait are shown in Fig. 3 (top panel, black and gray lines, respectively; see white dot in Fig. 4 for location). This location was chosen as representative of the interior Bass Strait, a region for which BRAN performs poorly (e.g., see Fig. 2). It is clear that $\breve{Y}_t$ is not a perfect predictor of Y_t. The mean SST is underpredicted by 0.4°C ($\overline{Y} = 15.1$°C and $\overline{\breve{Y}} = 14.7$°C). The seasonal cycle is reasonably well represented, although the trough-to-peak amplitude is low by 0.37°C and the minimum SST occurs approximately 17 days too early [correlation of $\rho = 0.972$ and root-mean-square error (RMSE) of 0.503°C, middle panel of Fig. 3]. The residual variability also compares poorly with the observations ($\rho = 0.488$) with an RMSE of 1.01°C (bottom panel of Fig. 3).

The linear statistical model described in section 3 was used to predict SST at 40°S, 147°E. The locations of $\breve{X}_t$ (the offshore predictor variables containing reliable oceanographic data to inform the inshore location boundary scaling) were chosen by finding the minima of the cost matrices defined in section 3. A different cost matrix is defined for the mean, the seasonal cycle, and the residual components. The details of the calculation of the cost matrices are shown here. The quality matrices are represented by point-by-point comparisons of $\breve{T}_{ijt}$ and T_{ijt} at each location (i, j) given by Eqs. (2)–(4). The **Q** metrics compare SST at the same point location and show the degree to which offshore locations can be trusted to provide accurate predictions of inshore mean SST (Fig. 4a), SST seasonal cycle (Fig. 4d), and SST residual variability (Fig. 4g). Accurate values of $\breve{T}_{ijt}$ are crucial to providing predictors of inshore SST variability.

The strength matrices are represented by a comparison between Y_t and T_{ijt} across the domain given by Eqs. (19)–(21). The **S** metrics show the degree to which offshore locations have a similar mean SST (Fig. 4b), SST seasonal cycle (Fig. 4e), and SST residual variability (Fig. 4h) as compared with the inshore location. A strong relationship between inshore and offshore SST is also crucial to providing a good predictor location. The proximity of the inshore and offshore locations is represented by **R**, an isotropic two-dimensional Gaussian function with a 20° length scale in both latitude and longitude [see Eq. (22), figure not shown]. This ensures that predictors are not chosen too far from the inshore location. An anisotropic Gaussian function could equally well be considered based on important length scales, but we use an isotropic form for simplicity and for concept demonstration.

The inverse of the product of these three fields gives the cost matrix [see Eq. (23) and Figs. 4c,f,i], the minimum of which corresponds to the location of $\breve{X}_t$ identified for use

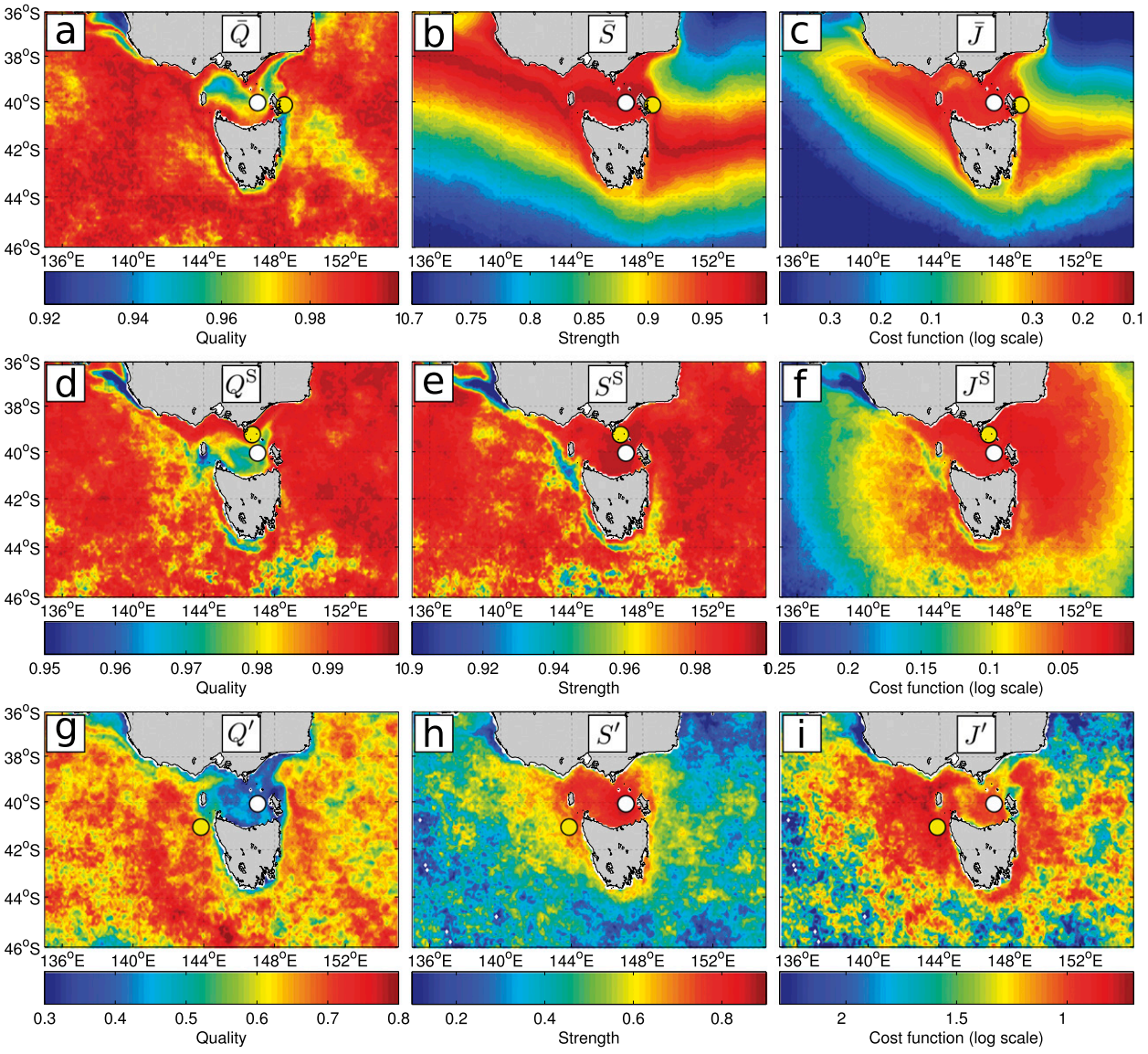

FIG. 4. (left) Quality, (center) strength, and (right) cost functions for (a)–(c) mean SST, (d)–(f) SST seasonal cycle, and (g)–(i) residual SST variability. The inshore location is shown by the white circle. The offshore locations that minimize the cost functions (the SST predictors) are shown by yellow circles.

in the statistical model. The offshore locations are indicated by yellow circles in Fig. 4 (note the different locations for the mean, seasonal cycle, and residual submodels). This procedure ensures that the chosen predictor is optimal based on our cost function criteria for estimating SST at that location, maximizes the relationship between the inshore and offshore locations, and is proximal in space.

The linear statistical model provides a substantially more accurate estimate of SST in Bass Strait ($\hat{Y}_t$) than BRAN SST ($\breve{Y}_t$). The mean is slightly overpredicted by 0.1°C ($\overline{Y} = 15.1$°C and $\overline{\hat{Y}} = 15.2$°C), which is a significant improvement over the 0.4°C underprediction given by $\overline{\breve{Y}}$. The seasonal cycle is better correlated ($\rho = 0.998$, a slight improvement of 0.026) and the RMSE has reduced by about two-thirds to 0.157°C. The residual variability is much better correlated ($\rho = 0.692$, an improvement of 0.204) and the RMSE has reduced by about half to 0.535°C. Time series of $\hat{Y}_t$, $\hat{Y}_t^S$, and $\hat{Y}_t'$ are shown in Fig. 3 (dashed lines). It is clear, from both the statistics quoted above and a visual comparison of the time series, that the statistical model provides better estimates of SST variability at this location in Bass Strait than are provided directly from BRAN.

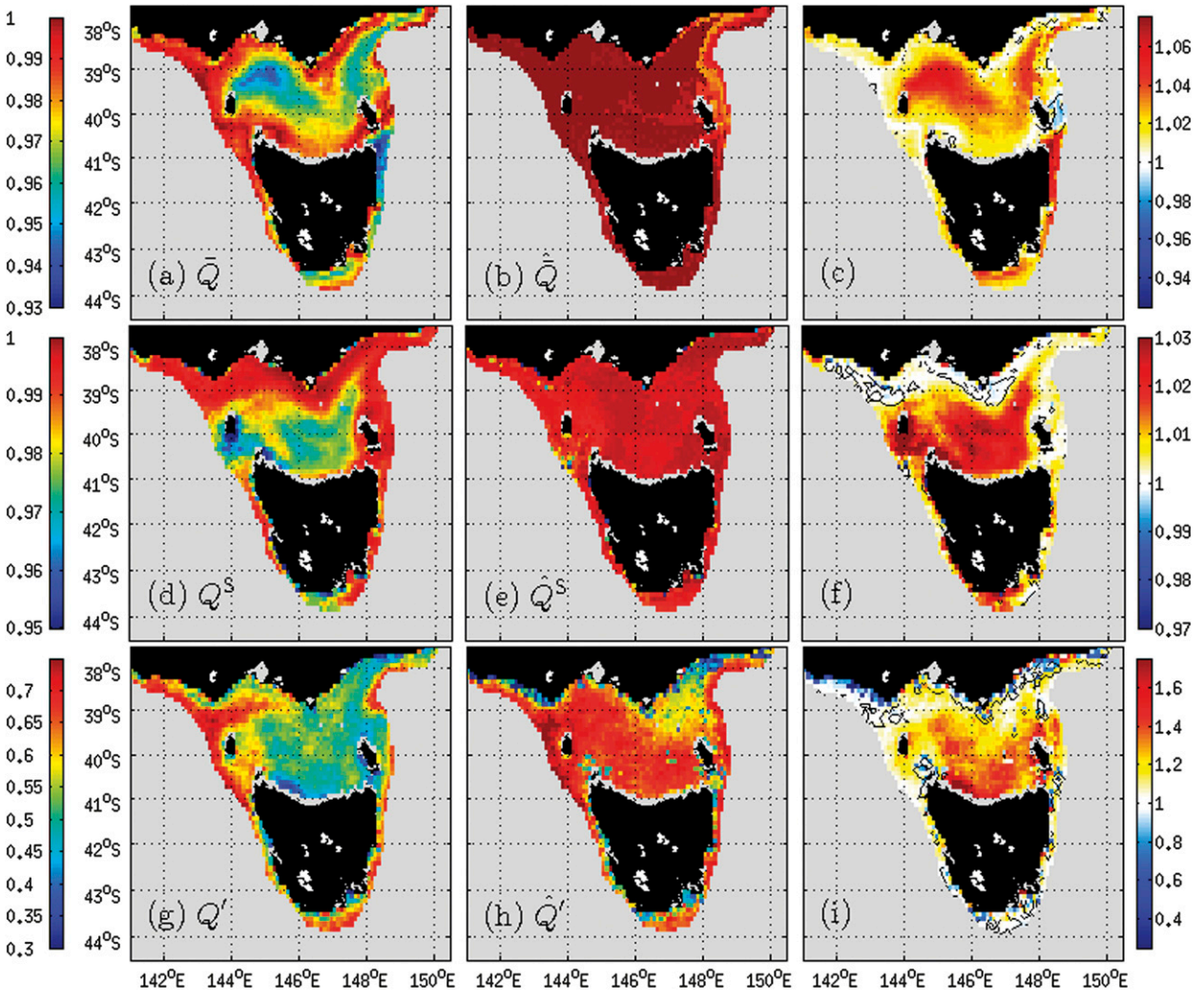

FIG. 5. A comparison of observed and predicted SST on the continental shelf around Tasmania and Victoria. The quality of (left) BRAN ($\mathbf{Q}$) and (center) predictions from the statistical model ($\hat{\mathbf{Q}}$) are shown for the (a)–(c) mean ($\overline{\mathbf{Q}}$ and $\hat{\overline{\mathbf{Q}}}$), (d)–(f) seasonal cycle ($\mathbf{Q}^S$ and $\hat{\mathbf{Q}}^S$) and (g)–(i) residual variability ($\mathbf{Q}'$ and $\hat{\mathbf{Q}}'$). (right) The improvement factors (the ratio of $\hat{\mathbf{Q}}$ and $\mathbf{Q}$). The black contour shows an improvement factor of exactly 1.

b. *Estimating SST across the continental shelf*

The approach described in the previous section (section 4a) was applied across the entire continental shelf. The statistical model was systematically applied to each location with water depths less than 200 m off the coasts of Victoria and Tasmania [section 4b(1)], the Great Australian Bight [section 4b(2)], and New South Wales and southern Queensland [section 4b(3)]. The cost function was masked for all locations in water depth less than 200 m to exclude those locations as potential predictors. The combined field of all $\hat{Y}_t$ over the continental shelf is denoted $\hat{\mathbf{T}}_t$. The analysis references the quality matrices calculated over these domains, which are shown in Figs. 5–7 as well as RMSEs, which are not shown.

1) TASMANIA AND VICTORIA

The model performs well at estimating SST on the continental shelf around Tasmania and Victoria. The quality matrix for the mean is shown in Fig. 5a. The $\overline{\mathbf{T}}$ are largely unrepresentative of SST in the interior of Bass Strait and near the coast of Tasmania, especially off the northeast coast. The quality function, recalculated using the estimate $\hat{\overline{\mathbf{T}}}$ from the statistical model, is shown in Fig. 5b. The statistical model provides improved estimates over most of the domain, especially where $\overline{\mathbf{T}}$ was a poor estimate, that is, in the interior Bass Strait and off the northeast coast of Tasmania (Fig. 5c). In these regions, the error between the observed and predicted mean is reduced by up to 1°C. The only region where $\hat{\overline{\mathbf{T}}}$ provides a worse

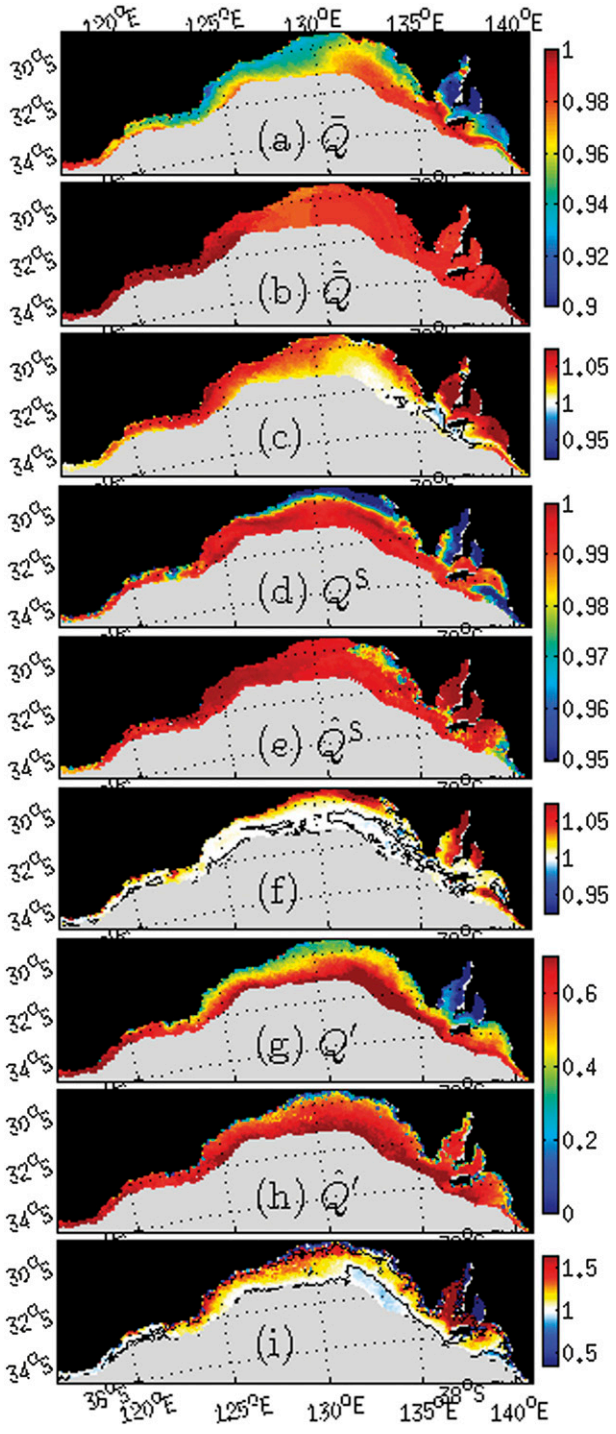

FIG. 6. A comparison of observed and predicted SST on the continental shelf around the GAB. The figure is divided into three sets with three panels each. Shown are (a),(d),(g) the quality of BRAN ($\mathbf{Q}$), (b),(e),(h) the quality of the predictions from the statistical model ($\hat{\mathbf{Q}}$), and (c),(f),(i) the improvement factors (the ratio of $\hat{\mathbf{Q}}$ and $\mathbf{Q}$) for (top three panels) the mean SST, (middle three panels) the seasonal cycle of SST, and (bottom three panels) the residual SST variability. The black contour shows an improvement factor of exactly 1.

estimate than $\breve{\bar{\mathbf{T}}}$ is to the east of Flinders Island. (It should be noted that this is a region where $\breve{\bar{\mathbf{T}}}$ provides a very good estimate and so it may be difficult to improve upon it.) Similarly, the model provides a much improved estimate of the SST seasonal cycle, especially in the interior Bass Strait and off the southern tip of Tasmania (Figs. 5d–f), where the RMSE is reduced by 60%–80% (up to 1°C). The residual SST variability is also much better represented by $\hat{\mathbf{T}}'_t$ than by $\breve{\mathbf{T}}'_t$, especially in Bass Strait (Figs. 5g–i). In the southern portion of the Bass Strait, the RMSE for the residual is reduced by up to 50% (0.5°C). However, the statistical model does not provide substantially improved estimates of residual SST immediately adjacent to most of the coastline, particularly Victoria and southern Tasmania. The $\hat{\mathbf{Q}}'$ also exhibits significant jumps in quality between adjacent points, indicating a lack of spatial smoothness in $\hat{\mathbf{T}}'_t$.

2) THE GAB

The model also provides substantially improved estimates of SST on the continental shelf around the Great Australian Bight (GAB). The quality matrix for the mean is shown in Fig. 6a. The $\breve{\bar{\mathbf{T}}}$ are largely unrepresentative of SST in the upper part of the GAB and in Spencer Gulf and Gulf St. Vincent (the gulfs). The quality function, calculated using $\hat{\bar{\mathbf{T}}}$, is shown in Fig. 6b. The statistical model provides improved estimates over almost the entire domain except near the mouths of the gulfs but, as before, this is a region where $\bar{\bar{\mathbf{T}}}$ provides a very good estimate with which to begin (Fig. 6c). The error in the prediction of the mean is reduced by up to 1°C over most of the domain and over 1.5°C in the gulfs. The model provides a much improved estimate of the SST seasonal cycle in the upper GAB and in the gulfs (Figs. 6d–f). The RMSE decreases away from the shelf break, reaching values up to 1°C (nearly a 100% reduction). The quality matrix for the residual variability $\mathbf{Q}'$ shows that BRAN performs poorly in the GAB away from the shelf break (Fig. 6g). Residual SST variability is much better represented by $\hat{\mathbf{T}}'_t$ in this region, except near the shelf break (again, where $\breve{\mathbf{T}}'_t$ is good to begin with) and immediately adjacent to the coast and in the upper part of the gulfs (Figs. 6h–i). The RMSE is reduced by 75%, up to 0.5°C, and higher in the gulfs (nearly 100%). As above, the $\hat{\mathbf{Q}}'$ also exhibits significant jumps in quality between adjacent points, indicating a lack of spatial smoothness in $\hat{\mathbf{T}}'_t$.

3) NEW SOUTH WALES AND SOUTHERN QUEENSLAND

Model performance on the continental shelf off New South Wales and Southern Queensland is more mixed than in the previous two regions. The quality matrix for the mean is shown in Fig. 7a. The statistical estimates

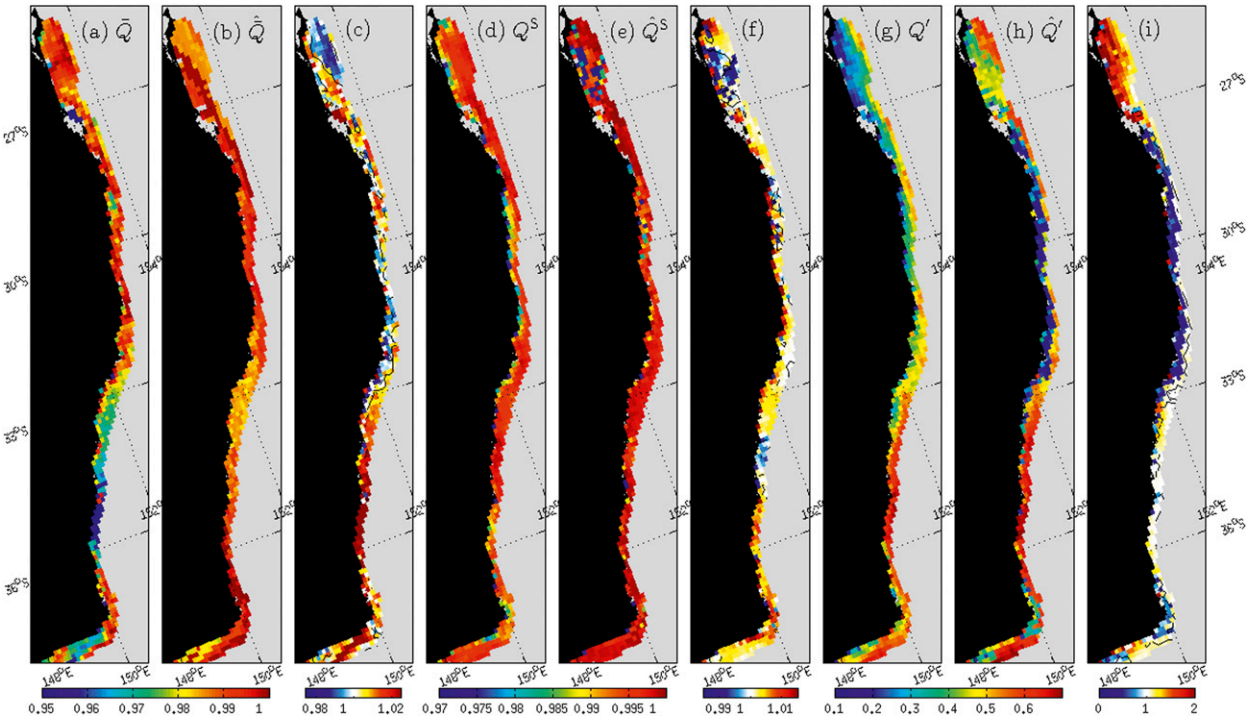

FIG. 7. As in Fig. 6, but a comparison of observed and predicted SST on the continental shelf around New South Wales and southern Queensland. Note that the orientation of the panels has changed from Fig. 6 because of the projection of the location.

$\hat{\bar{\mathbf{T}}}$ are generally better than $\breve{\bar{\mathbf{T}}}$ south of approximately 33°S, but the results are mixed north of about 33°S and quite poor off of Fraser Island in the Coral Sea (Figs. 7b–c). Similarly, the statistical model provides a much improved estimate of the SST seasonal cycle, except near the Coral Sea and in a region around 34.5°S, where the results are very mixed (Figs. 7d–f). The RMSEs are up to 0.25°C for the seasonal cycle and up to 0.4°C for the residual, and they increase shoreward (away from the shelf break) in both cases. The residual variability is much better represented by $\hat{\mathbf{T}}'_t$ than by $\breve{\mathbf{T}}'_t$ in the Coral Sea region (north of ~27°S), is poorly represented between this region and about 33°S, and displays mixed results south of approximately 33°S (Figs. 7g–i). These results indicate three clearly defined domains: (i) near the Coral Sea (north of ~27°S), (ii) between around 27° and 33°S, and (iii) south of approximately 33°S. The differences between these three domains are clearly visible in the statistical model results for the residual variability submodel (Fig. 7, three rightmost panels). It is interesting to note that around 33°S is roughly the latitude at which the EAC separates from the coast (Godfrey et al. 1980). This likely corresponds to the different physical processes acting to the north and south of this separation point, a factor that might be important in model performance depending on physical process complexity and scale issues.

5. Connectivity with the mean circulation

An analysis of the optimal locations of the offshore predictors based on our previous criteria was also performed. The continental shelf around Tasmania and Victoria was chosen as the case study region. The shelf was divided into five regions (northwest, northeast, Bass Strait, western Tasmania, and eastern Tasmania), and these have been color coded along with the corresponding offshore predictor locations from the model for residual SST variability (see Fig. 8, top panel). Predictors tend to lie either (i) along the shelf break immediately adjacent to the inshore region that they predict or (ii) offshore and predominantly to the west (~84% of all predictors in this region lie to the west of the southern tip of Tasmania). The predictors also tend to lie in regions where the mean surface flow, determined from daily fields of meridional and zonal surface currents from BRAN, is strong and continuous between the shelf and the offshore region (see Fig. 8, top panel, gray arrows). This suggests that connectivity between the shelf and offshore regions may be a useful physically based metric for optimal predictor selection.

Connectivity was determined by calculating the Lagrangian trajectories of particles, seeded at an offshore location, following the mean flow: $\mathbf{x}(t) = [x_1(t)\ x_2(t)]^{\mathrm{T}}$.

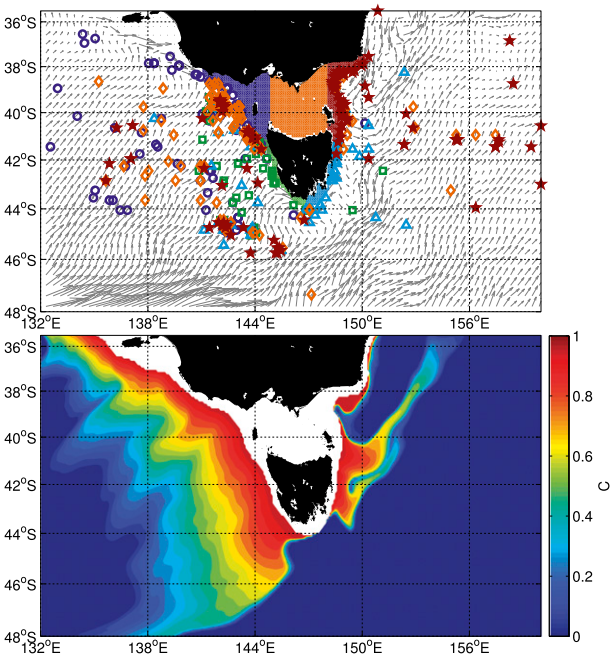

FIG. 8. Off-shore predictor locations and connectivity information. (top) The shelf is divided into five regions (northwest, northeast, Bass Strait, western Tasmania, and eastern Tasmania), and these have been color coded along with the corresponding offshore predictor locations from the model for residual SST variability. (bottom) The **C** calculated from Lagrangian particle trajectories [Eq. (26)].

Given a location at time t, the location at some time Δt later can be approximated by

$$\mathbf{x}(t+\Delta t) = \mathbf{x}(t) + \mathbf{u}[\mathbf{x}(t)]\Delta t, \tag{24}$$

where $\mathbf{u}(\mathbf{x})$ is the mean flow at location $\mathbf{x}$. Similarly, the trajectories backward in time can be approximated by

$$\mathbf{x}(t-\Delta t) = \mathbf{x}(t) - \mathbf{u}[\mathbf{x}(t)]\Delta t. \tag{25}$$

The mean flow was calculated from BRAN at fixed locations in space across the $^1/_{10}°$ grid and so the mean flow $\mathbf{u}$ at the exact location $\mathbf{x}(t)$ was determined by bilinear interpolation. In our algorithm, trajectories stop moving if they reach the coast or the open boundaries. Trajectories forward and backward in time starting from the same initial location are denoted $\mathbf{x}_f(t)$ and $\mathbf{x}_b(t)$, respectively. To simulate turbulent motion, we add a random kick to the particles at each time step by replacing $\mathbf{u}(\mathbf{x})$ with $\mathbf{u}(\mathbf{x}) + \Delta\mathbf{u}$. The random kick velocity $\Delta\mathbf{u}$ is a Gaussian random number with a mean of zero and a standard deviation given by $\sqrt{2A_h/\Delta t}$, where A_h is a horizontal eddy diffusivity (e.g., Brickman and Smith 2002).

The connectivity statistic **C**, measuring the extent of connectivity between each of the offshore locations and the continental shelf, is calculated from

$$C_{ij} = 2\min\left(1 - \frac{\tau_{200,ij}}{\tau}, 0.5\right), \tag{26}$$

where $\tau_{200,ij}$ is the total time spent over the continental shelf (water depth less than 200 m) by both $\mathbf{x}_f(t)$ and $\mathbf{x}_b(t)$ starting from an initial location (i, j) and integrated for a total T. If a trajectory spends the entire time on the shelf, either backward or forward, then $C_{ij} = 1$, and if it never reaches the shelf, then $C_{ij} = 0$; otherwise, $0 < C_{ij} < 1$. Connectivity around Tasmania and Victoria was calculated for each location in the domain bounded by 35°–48°S and 132°–160°E. An ensemble of 500 forward and backward trajectories (with $\tau = 300$ days, e.g., 150 days forward and 150 days backward; $\Delta t = 0.5$ days; $A_h = 4\,\mathrm{m^2\,s^{-1}}$) was calculated at each location to yield 500 connectivity matrices [calculated according to Eq. (26)], which were then averaged at each location to give the final **C** (Fig. 8, bottom panel).

The statistical model was applied over the continental shelf of Tasmania and Victoria, with the cost function (used for determining offshore predictor locations) modified as follows:

$$J_{ij} = \frac{1}{Q_{ij}S_{ij}R_{ij}C_{ij}}, \tag{27}$$

to include the effect of **C**. The quality functions calculated using the new estimate of $\hat{Y}_t$ are shown in the middle panels of Fig. 9. The inclusion of the connectivity matrix improves the model predictions in two ways. First, the results are much smoother in space; for example, there are fewer jumps in quality between adjacent grid points. Second, the quality functions indicate that the model predictions perform better (especially for the seasonal cycle and residual variability) than those without the connectivity information (cf. right panels of Figs. 5, 9). Notably, the results for residual SST variability along coastal Victoria are much improved. It should be noted that the results for the mean SST do not show such a dramatic improvement and in some regions are slightly worse. This may be because information about the mean circulation is implicitly part of the mean SST statistics, and so its inclusion does little to improve mean SST predictions.

By including the connectivity as an integral part of the model, we have moved from a purely statistical model to a hybrid statistical–connectivity model. The power of such a model is that changes in the connectivity (e.g., under a changing climate) can be incorporated into the model to modify it accordingly. This concept can be generalized to a statistical–dynamical model in which

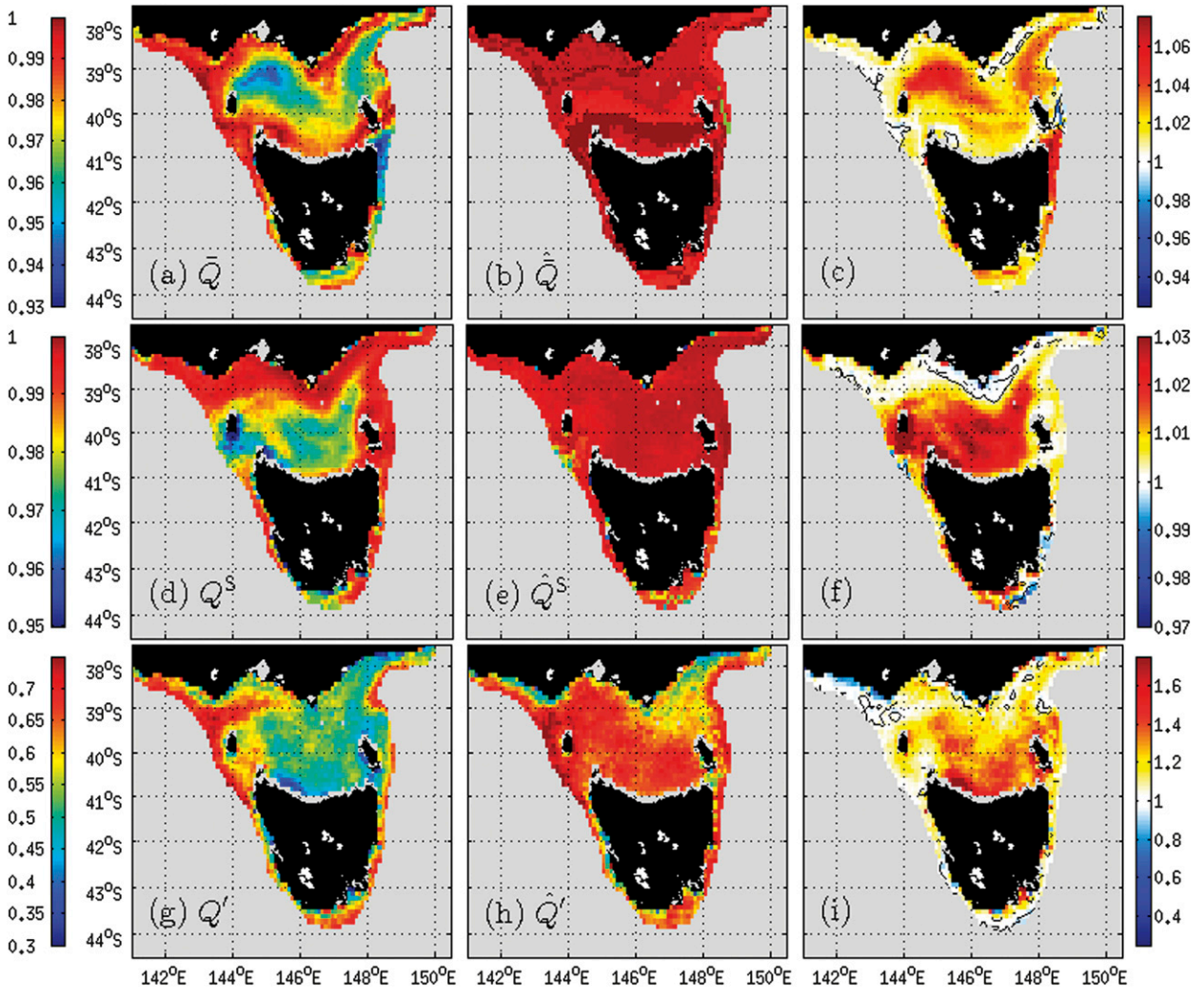

FIG. 9. As in Fig. 5, except the statistical model includes the shelf–offshore connectivity information introduced in section 5.

information related to ocean dynamics (in our case, only mean circulation) are explicitly incorporated into the statistical model.

6. Conclusions and future work

The approach presented in this paper provides a systematic statistical method for the estimation of across-shelf ocean climate variability (here, the case study of sea surface temperature in an Australian marine context was presented) across a range of time scales. The mean SST, SST seasonal cycle, and residual SST variability on the shelf were predicted using estimates of offshore SST from an ocean reanalysis product (BRAN). Independent linear statistical models were developed to predict each of these components, and the model parameters were informed using the observed (e.g., from AVHRR) relationship between SST offshore and SST on the continental shelf. A method of optimally choosing the offshore predictor using three criteria (data quality, strength of offshore/shelf connection, and proximity) was developed. Finally, the model was refined into a simple hybrid statistical–connectivity model by including passive tracer connectivity, based on the mean surface circulation, as a further criterion for predictor selection. The approach presented in this paper represents a potentially useful method for generating homogeneous daily SST fields on the continental shelf and provides a framework for estimating other climate fields (e.g., sea surface salinity and surface chlorophyll a) at relatively low computational cost.

The model was applied to the continental shelf around southeastern Australia. The statistical model predictions of across-shelf SST are generally much closer to the observations than those available directly from BRAN—especially around Tasmania, Victoria, and the Great Australian Bight. The mean and seasonal cycle are much better

predicted. Typical RMSEs for the seasonal cycle were reduced by up to 1°C (60%–80% reduction in Bass Strait and nearly 100% reduction in the Great Australian Bight). The residual variability was also better predicted, except very near to the coast. The RMSEs in central Bass Strait and the upper Great Australian Bight are demonstrably reduced by 0.5°C (50% reduction in Bass Strait and 75% reduction in the Great Australian Bight). Prediction quality for coastal New South Wales and southern Queensland were more mixed, and it is not clear that the statistical model provides better predictions in those regions. Overall, however, our model shows significant promise as a methodological approach for the estimation of across-shelf SST in terms of accuracy, robustness, and potential utility beyond the Australian case study example.

In the simplest statistical model approach, predictor locations were identified by minimizing a cost function depending first on three factors: quality, strength, and proximity. We do not presume that this is an exhaustive list of factors that would influence the choice of predictors. They were selected here based on a combination of intuition and oceanographic understanding and allowed us to develop a relatively simple model. The inclusion of other relevant factors in the analysis, once identified, would be relatively simple as an addition to the model formulation. For example, we have been able to readily expand the definition of the cost function to also include a simple measure of connectivity, creating a hybrid type of statistical–connectivity model.

Connectivity between the shelf and the open ocean is defined in terms of Lagrangian trajectories, given the mean surface circulation. We found that predictors that lie in regions with strong connectivity to the coast provided accurate and spatially smooth results. While a purely statistical approach, such as localized EOF analysis, could also lead to model improvements, our connectivity-based approach has the strength of a hybrid statistical–physical model, in that we are informed about from where the information is coming. However, the connectivity statistics should be improved with a more complete treatment and consideration of the full three-dimensional and time-varying flow field, and not only the mean flow. These connectivity statistics could be calculated by extending our technique appropriately, or they could be obtained, for example, from projects such as the Marine Connectivity Interface (Connie2, http://www.csiro.au/connie2/; Condie et al. 2011). We chose to use the mean circulation as the connectivity metric of relevance in our demonstration of concept study here since analysis of the predictor locations indicated that, to first order, it was the physically based oceanographic feature (i.e., the circulation) that linked SST variability between the shelf and offshore regions. It is clear that the inclusion of this physically based metric provided improved model results and greater spatial robustness of the model predictions.

It may be possible to further refine the model by considering frequency-dependent models of residual variability. The ''gappy'' nature of the observed SST time series prevents the application of a fully spectral approach, but this could be partly achieved by splitting the residual variability into more than one time series. For example, monthly means of the residual variability could be calculated and this time series would represent the ''low frequency'' residual variability. The remainder would represent the ''high frequency'' residual variability. It is possible that different mechanisms are at play on different time scales. Separate models for each could then be constructed, allowing for different predictor locations and regression coefficients. Additionally, other predictors could be included in the model (local winds, climate modes of variability, etc.), as it is likely that different mechanisms may lead to predictability on different time scales. Seasonally dependent regression coefficients may also improve the residual SST prediction.

A possible weakness of the statistical model is that each submodel is informed by a single offshore location. A more complex model version might instead utilize information from multiple locations to inform each inshore SST prediction. There are several ways in which this could be achieved. For example, the residual could be predicted by multiple linear regression, with the offshore predictors selected to maximize the amount of on-shelf variance explained. A more general approach would be to use kernel regression, with the kernel defined in a similar way to the cost matrix. This could then be generalized to the submodels for the mean and seasonal cycle (which are not presented as simple linear regression models).

Acknowledgments. The AVHRR data were provided by the Group for High Resolution SST (GHRSST) and the U.S. National Oceanographic Data Center. The authors thank Matthew Chamberlain and Simon Wotherspoon for the helpful discussions. The authors acknowledge funding from the Australian Research Council Super Science Fellowship (Grant FS110200029). The authors also acknowledge the two anonymous reviewers for their helpful and insightful comments.

APPENDIX A

Estimating the Seasonal Cycle by Harmonic Regression

Given a time series x_t, assume that its seasonal cycle x_t^S can be approximated by a sum of K harmonics of the annual cycle:

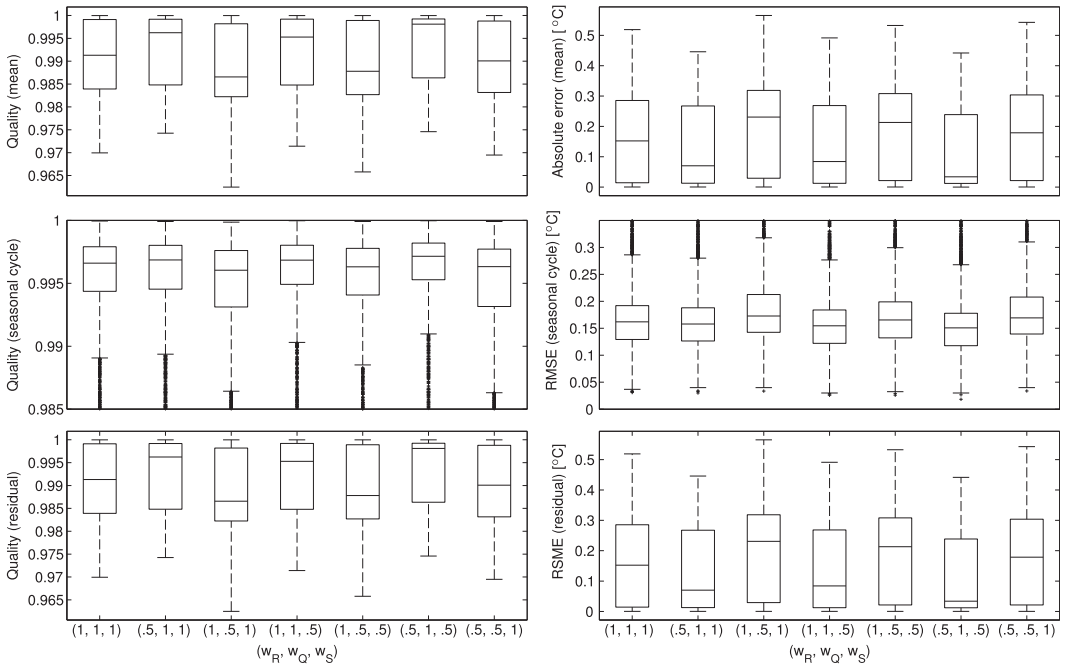

FIG. B1. Sensitivity tests of the boundary-scaling model to relative weighting of the terms that make up **J** [Eq. (B2)]. (left) The quality functions and (right) the errors for the (top) mean SST, (middle) SST seasonal cycle, and (bottom) residual SST variability for the relative weighting of **Q**, **S**, and **R** given by the triplet of values (w_Q, w_S, w_R). For each sensitivity test, the results (quality values and errors) at all locations on the shelf are collected and summarized by its probability distribution (represented here as a box-and-whisker plot that indicates the four quartiles along with any outliers).

$$x_t^S \simeq \sum_{k=1}^{K} A_k \cos(\omega_k t - \phi_k), \tag{A1}$$

where A_k, ϕ_k, and ω_k are the amplitude, phase, and frequency of the kth harmonic, respectively. The ω_k are written as

$$\omega_k = 2\pi k L, \tag{A2}$$

where L is the length of the year (in units of the sample rate of x_t, for example, $L = 12$ for monthly data). These frequencies correspond to a period of 1 yr for $k = 1$, 1/2 yr for $k = 2$, 1/3 yr for $k = 3$, etc. Note that Eq. (A1) is equivalent to

$$x_t^S \simeq \sum_{k=1}^{K} (a_k \cos\omega_k t + b_k \sin\omega t), \tag{A3}$$

where $A_k^2 = a_k^2 + b_k^2$ and $\phi_k = \arctan(b_k/a_k)$. We use $K = 3$ in this study.

We write the following regression model:

$$x_t = \boldsymbol{\mathcal{B}}\mathbf{s}_t + \varepsilon_t, \tag{A4}$$

where $\boldsymbol{\mathcal{B}}$ is a vector of length $2K$ of regression coefficients, $\mathbf{s}_t$ is a vector of length $2K$ of sines and cosines, and ε_t is an error term representing effects not included in the model. The ith element of $\mathbf{s}_t$ is given by:

$$\text{for} \quad \text{odd}\, i, \quad s_{it} = \cos\omega_k t, \quad \text{where} \quad k = (i+1)/2, \tag{A5}$$

and

$$\text{for} \quad \text{even}\, i, \quad s_{it} = \sin\omega_k t, \quad \text{where} \quad k = i/2. \tag{A6}$$

The estimated regression coefficients $\hat{\boldsymbol{\mathcal{B}}}$ are calculated by least squares. The values of a_k and b_k are given by the $(2k-1)^{\text{th}}$ and $(2k)^{\text{th}}$ element of $\hat{\boldsymbol{\mathcal{B}}}$, respectively. It is then trivial to calculate A_k and ϕ_k using the relations given above.

APPENDIX B

Cost Function Sensitivity to Relative Weightings of Terms

In the model described in section 3, the optimal predictor location is determined by the minimum of **J** given by Eq. (23):

$$J_{ij} = \frac{1}{Q_{ij} S_{ij} R_{ij}}. \tag{B1}$$

In this form, the individual terms (**Q**, **S**, and **R**) are each weighted equally. Here, we consider another form in which each term is given a weight indicating its overall contribution to the cost function:

$$J_{ij} = \frac{1}{[w_Q Q_{ij} + (1 - w_Q)][w_S S_{ij} + (1 - w_S)][w_R R_{ij} + (1 - w_R)]}. \quad \text{(B2)}$$

Here, w_Q, w_S, and w_R are scalar values constrained to lie between 0 and 1. A value of 1 gives full weighting to that term and a value of 0 gives no weighting to that term. For example, weighting values of $(w_Q, w_S, w_R) = (1, 0.5, 0.2)$ would give full weighting to the quality, 50% weighting to the strength, and 20% weighting to the localization.

A suite of sensitivity calculations were performed to test the sensitivity of the boundary-scaling model to the relative weighting of the terms in the cost function. For each sensitivity test, the model was fit to the entire continental shelf around the Great Australian Bight, Tasmania, Victoria, New South Wales, and southern Queensland (as in section 4), and the quality values and RMSEs at all grid points were collected together, summarized by their probability distribution (Fig. B1). There were small variations in the mean and spread of the results for different weighting choices, which indicated that the quality appears to be the most important term and localization the least important term (in the sense that these results improve as these terms are weighted higher and lower, respectively). However, considering the overlap in the spread of quality values and RMSEs across all sensitivity runs, including the equally weighted model with $(w_Q, w_S, w_R) = (1, 1, 1)$, we can conclude that the results are not strongly sensitive to changes in the relative weighting of the three terms. Therefore, in the interest of simplicity, we have elected to weight all the terms equally.

REFERENCES

ABS, 2001: Regional population growth, Australia and New Zealand. Australia Bureau of Statistics Catalog 3218.0, 99 pp.

Benestad, R., I. Hanssen-Bauer, and D. Chen, 2008: *Empirical-Statistical Downscaling.* World Scientific Publishing Company, 228 pp.

Brickman, D., and P. Smith, 2002: Lagrangian stochastic modeling in coastal oceanography. *J. Atmos. Oceanic Technol.,* **19,** 83–99.

Christensen, O., J. Christensen, B. Machenhauer, and M. Botzet, 1998: Very high-resolution regional climate simulations over Scandinavia—Present climate. *J. Climate,* **11,** 3204–3229.

Condie, S., J. Mansbridge, and M. Cahill, 2011: Contrasting local retention and cross-shore transports of the East Australian Current and the Leeuwin Current and their relative influences on the life histories of small pelagic fishes. *Deep-Sea Res. II,* **58,** 606–615.

Corney, S., and Coauthors, 2010: Climate futures for Tasmania: Climate modelling. Antarctic Climate and Ecosystems Cooperative Research Centre Tech. Rep., 81 pp.

Fuller, W. A., 1987: *Measurement Error Models.* Wiley Series in Probability and Statistics, Wiley, 440 pp.

Giorgi, F., 1990: Simulation of regional climate using a limited area model nested in a general circulation model. *J. Climate,* **3,** 941–963.

Godfrey, J., G. Cresswell, T. Golding, A. Pearce, and R. Boyd, 1980: The separation of the East Australian Current. *J. Phys. Oceanogr.,* **10,** 430–440.

Guo, X., H. Hukuda, Y. Miyazawa, and T. Yamagata, 2003: A triply nested ocean model for simulating the Kuroshio—Roles of horizontal resolution on JEBAR. *J . Phys. Oceanogr.,* **33,** 146–169.

Hellstrom, C., D. Chen, C. Achberger, and J. Raisanen, 2001: Comparison of climate change scenarios for Sweden based on statistical and dynamical downscaling of monthly precipitation. *Climate Res.,* **19,** 45–55.

Hobday, A., J. Hartog, J. Middleton, C. E. Teixeira, J. Luick, R. Matear, and S. Condie, 2011: Understanding the biophysical implications of climate change in the southeast—Modelling of physical drivers and future changes. FRDC Rep. 2009/056, Fisheries Research and Development Corporation and CSIRO Marine and Atmospheric Research, 99 pp.

Holbrook, N., and N. Bindoff, 2000: A statistically efficient mapping technique for four-dimensional ocean temperature data. *J. Atmos. Oceanic Technol.,* **17,** 831–846.

Huth, R., 2002: Statistical downscaling of daily temperature in central Europe. *J. Climate,* **15,** 1731–1742.

Murphy, J., 1999: An evaluation of statistical and dynamical techniques for downscaling local climate. *J. Climate,* **12,** 2256–2284.

Oey, L., and P. Chen, 1992: A nested-grid ocean model: With application to the simulation of meanders and eddies in the Norwegian coastal current. *J. Geophys. Res.,* **97** (C12), 20 063–20 086.

Oke, P. R., and A. Schiller, 2007: Impact of Argo, SST, and altimeter data on an eddy-resolving ocean reanalysis. *Geophys. Res. Lett.,* **34,** L19601, doi:10.1029/2007GL031549.

——, G. Brassington, D. Griffin, and A. Schiller, 2008: The Bluelink Ocean Data Assimilation System (BODAS). *Ocean Modell.,* **21,** 46–70.

Oliver, E. C. J., 2011: Local and remote forcing of the ocean by the Madden-Julian oscillation and its predictability. Ph.D. thesis, Dalhousie University, 180 pp.

Palutikof, J., C. Goodess, S. Watkins, and T. Holt, 2002: Generating rainfall and temperature scenarios at multiple sites: Examples from the Mediterranean. *J. Climate,* **15,** 3529–3548.

Priestley, M. B., 1981: *Spectral Analysis and Time Series.* Academic Press, 890 pp.

Qian, B., J. Corte-Real, and H. Xu, 2002: Multisite stochastic weather models for impact studies. *Int. J. Climatol.,* **22,** 1377–1397.

Ridgway, K., J. Dunn, and J. Wilkin, 2002: Ocean interpolation by four-dimensional weighted least squares—Application to the waters around Australasia. *J. Atmos. Oceanic Technol.,* **19,** 1357–1375.

Schiller, A., P. Oke, G. Brassington, M. Entel, R. Fiedler, D. Griffin, and J. Mansbridge, 2008: Eddy-resolving ocean circulation in the Asian–Australian region inferred from an ocean reanalysis effort. *Prog. Oceanogr.,* **76,** 334–365.

Trapp, R., B. Halvorson, and N. Diffenbaugh, 2007: Telescoping, multimodel approaches to evaluate extreme convective weather under future climates. *J. Geophys. Res.,* **112,** D20109, doi:10.1029/2006JD008345.

von Storch, H., and F. Zwiers, 2002: *Statistical Analysis in Climate Research.* Cambridge University Press, 484 pp.

——, E. Zorita, and U. Cubasch, 1993: Downscaling of global climate change estimates to regional scales: An application to Iberian rainfall in wintertime. *J. Climate,* **6,** 1161–1171.

Wang, X. L., V. R. Swail, and A. Cox, 2010: Dynamical versus statistical downscaling methods for ocean wave heights. *Int. J. Climatol.,* **30,** 317–332.

Wilby, R., T. Wigley, D. Conway, P. Jones, B. Hewitson, J. Main, and D. Wilks, 1998: Statistical downscaling of general circulation model output: A comparison of methods. *Water Resour. Res.,* **34,** 2995–3008.

Wilks, D., 1999: Multisite downscaling of daily precipitation with a stochastic weather generator. *Climate Res.,* **11,** 125–136.

Zhang, X., Y. Lu, K. Thompson, J. Jiang, and H. Ritchie, 2010: Tropical Pacific Ocean and the Madden-Julian oscillation: Role of wind and buoyancy forcing. *J. Geophys. Res.,* **115,** C05022, doi:10.1029/2009JC005734.

Zorita, E., and H. von Storch, 1999: The analog method as a simple statistical downscaling technique: Comparison with more complicated methods. *J. Climate,* **12,** 2474–2489.